IEEE Access
Multidisciplinary ⋮ Rapid Review ⋮ Open Access Journal

Received 25 November 2022, accepted 14 January 2023, date of publication 25 January 2023, date of current version 30 January 2023.

Digital Object Identifier 10.1109/ACCESS.2023.3239584

RESEARCH ARTICLE

Remaining Shelf-Life Estimation of Fresh Fruits and Vegetables During Transportation

ARWA ABOUGHARIB, MAHMOUD AWAD, AND MALICK NDIAYE
Department of Industrial Engineering, American University of Sharjah, Sharjah, United Arab Emirates

Corresponding author: Arwa Abougharib (arwa.momen96@gmail.com)

This work was supported in part by the American University of Sharjah Smart City Research Institute Grant SRC-18, and in part by the Open Access Program from the American University of Sharjah.

ABSTRACT During transportation, prediction of the Remaining Shelf-Life (RSL) of Fresh Fruits and Vegetables (FFVs) is critical for planning and quality cost estimation. The Internet of Things (IoT) enables measured environmental variables to be processed in real-time. However, there is a need for a validated, real-time computational method that translates environmental measurements to dynamic RSL estimates. Most existing generic RSL models for FFVs are qualitative, invasive, or static. This study establishes a generic RSL model for FFVs under dynamic and unplanned logistic conditions. The model is based on estimating the current rate of general decay based on the expected respiration rate of the product, and integrating the decay rate with respect to time. Its implementation is non-destructive, non-invasive, and does not require accelerated shelf-life experiments before deployment. In addition, since the original model is rather computationally intensive, a surrogate model was proposed to allow the model to be implemented in fast, real-time applications for 'Edge IoT.' Experimental validation of the model using three fresh products (strawberries, apricots, and spinach) in a domestic refrigerator resulted in a maximum deviation of 1.3 days in prediction error using the original model and 2.95 days using the surrogate model. Nonetheless, the predictions made using either the original or surrogate models were statistically sound and not significantly different from the observed shelf lives of the samples, even at the 0.01 significance level.

INDEX TERMS Remaining shelf life, fresh fruits and vegetables, IoT, food supply chain, quality monitoring, transportation.

I. INTRODUCTION

The waste of Fresh Fruits and Vegetables (FFVs) is a significant issue in food supply chain industries. Srivastava et al. [1] reported that food retailers experience profit margin losses due to cold chain risks such as transport delays and breakdowns, temperature abuse, and cross-contamination. Food losses are a burden to society, too, with one-third of all edible human food wasted annually [2].

It is well known that temperature variability is inevitable across the supply chain and that in the case of fresh products, degradation reactions are accelerated at temperatures above the recommended storage temperatures. Therefore, temperature variability must be accounted for when estimating the product's RSL at any point in the chain. IoT makes it possible to measure environmental parameters such as temperature and humidity during transit and communicate these measurements in real-time to the cloud [3] for quality monitoring and real-time fleet routing optimization [4]. The product's RSL can be estimated in real time with a suitable computational method. A mathematical model that accepts the measured environmental parameters and outputs the RSL for a given product in real time is thus pivotal to the success of such advanced decision systems.

Predicting the shelf-life of sealed, dried, highly processed, and chemically-preserved foods is well understood and established with simple and reliable mathematical models. On the other hand, predicting the shelf-life of unsealed, unprocessed, and biologically active foods (such as fresh fruits and vegetables, milk, fish, and meat) shipped together with other types of fresh foods under chaotic logistic conditions remains a largely divisive and elusive problem. This is not due to the

The associate editor coordinating the review of this manuscript and approving it for publication was Giambattista Gruosso.

This work is licensed under a Creative Commons Attribution-NonCommercial-NoDerivatives 4.0 License.
For more information, see https://creativecommons.org/licenses/by-nc-nd/4.0/

lack of complex mathematical models that cater to the main decay factors of such foods. Rather, the numerous limitations, high specificity to a food species, and the need for destructive tests and/or time-consuming pre-tests render current theoretical models unsustainable in practice.

In this paper, we present a new, real-time, non-destructive, highly generalizable computational method to predict the remaining shelf-life of FFVs under unplanned logistic conditions. The method uses real-time measurements of temperature and humidity and - most significantly - precludes the need for characterization pre-tests as it is initialized with only well-documented and easily accessible thermophysical properties of the product. Moreover, the proposed model has been validated with three types of FFVs under various packaging conditions and frequencies of temperature disruptions.

II. LITERATURE REVIEW

During circulation, it cannot be guaranteed that the product's recommended storage temperature requirements will always be met. Consequently, the problem of shelf-life reduction due to deviation from the recommended storage conditions has long been of interest to the food science community. There are five types of decay in relation to FFVs: Preharvest biological decay, senescence, microbiological decay, chemical deterioration, and physical degradation [5].

Despite the temperature and headspace gas composition being just two of many sources of degradation of fresh produce, they are still considered major predictors of post-harvest degradation and distribution losses [6]. As a result, temperature and gas measurements can be used to provide an optimistic prediction of the RSL. All other sources of decay, such as vibration and moisture loss, can be ignored if they are not significantly different from the logistic conditions under which the initial shelf-life was estimated.

Hence, for all future discussions, we shall use the word 'decay' to refer to the amalgamation of all post-harvest, undesirable quality changes that are affected by temperature and/or atmospheric composition, namely: Senescence, chemical deterioration, and microbiological decay.

In their review, Hertog et al. [7] categorized the modeling approaches for warehouse management into three groups, all of which use the measured environmental conditions along the cold chain. Namely, Statistical Process Control (SPC), specific quality attribute models, and generic shelf-life models. SPC models focus on monitoring and correcting environmental conditions, while specific attribute models monitor a single biochemical attribute over time. The most comprehensive approach is the generic shelf-life model, where the product's shelf-life is determined considering not only a limiting quality attribute of the product but also its respiration activity and moisture loss. We are interested in the second and third approaches, as they output an RSL estimate: An actionable piece of information based on which the storage, sales, and distribution of perishable products can be optimized, as opposed to a binary (Keep/Discard) recommendation from an SPC model.

Most well-known mathematical models of shelf-life traditionally fall into the second category (specific quality attribute models), consisting of a primary kinetic model and one or more secondary models. The primary model consists of one or more differential equations relating the rate of change of the food quality index to time, while a secondary model relates the rate of change of the food quality index to degradation factors other than time, such as temperature, pH, water activity, etc. The evolution of the shelf-life (defined in terms of a food quality index) is found by integrating the differential equations in the primary and secondary models over time.

To develop a kinetic model of food degradation, a measurable physical, biological, chemical, or sensory property of the food that strongly correlates with loss of quality and customer acceptance, Q, is first defined, then experimentally measured for different storage temperatures and times. Afterward, the relationship between Q and storage time t at a constant temperature T is fitted with either a straight-line on a linear plot or a semi-log plot of the data points, whichever is the best fitting. The differential of this line is of either zero-order or first-order, based on which the overall kinetics of decay are classified as either zero-order or first-order kinetics, respectively, and the reaction rate constant k is found at that specific temperature T. The reaction rate constant k is often a function of the storage temperature T, thus the need for a secondary model to account for the effect of temperature on the rate constant k.

The Arrhenius relationship has been widely used to model the reaction rate constant, k with respect to T. Eventually, a specific quality attribute model considers a product to have reached its shelf-life when the quality index Q reaches a predefined acceptability limit.

Despite the overwhelming popularity of using traditional zero-, first-, and second-order kinetics to model degradation in fresh and horticultural products, [8] asserted that most food degradation processes do not follow any standard kinetic model and that shelf-life estimation need not assume a kinetic model order a priori. Another drawback of using fixed-order kinetics is that the change in the limiting quality attribute is often due to multiple biochemical reactions which are not necessarily of the same order. Moreover, several models of different order might fit the data points equally well, resulting in the reaction order not being clearly defined and possibly, the selection of an inaccurate model that systematically over - or underestimates the shelf-life [5], [8].

The equally popular Arrhenius model has been classically used as a secondary model for microbial growth and, consequently, food deterioration models. However, its widespread adoption has also been greatly criticized. It is perfectly appropriate for predicting the rate of reactions between gases in solutions, but ''makes no sense at all in the description of microbial growth kinetics'' [9, p. 932], for several reasons, including but not limited to: The temperature-independence of the activation energy, the model's inability to account for optimal growth temperature, the irrelevance of the

Universal Gas Constant R, and (in microbial growth models specifically), the cumbersome reference to a mol of bacteria (which would weigh 600,000 metric tons), and that it attempts to model the number of microbial cells or their growth rate, which is fundamentally different than modeling the concentration of a chemical reactant.

Furthermore, [10] reviewed the appropriateness of the Arrhenius and two other widely-used secondary models, namely, the Eyring-Polanyi and WLF models, both of which were -like the Arrhenius model- originally derived for non-food systems, and pointed out that a model's good fit alone does not assure its validity. They demonstrated that using those three classical models in the context of food deterioration is theoretically flawed and that their parameters should not be given any physical meaning.

Overall, determining kinetic model constants typically requires tedious accelerated shelf-life studies that must be conducted for each unique combination of food type, quality index, and packaging. Nonetheless, the best quality index to be used as a predictor of deterioration can be different for each product, and - for the same product- differ for isothermal versus non-isothermal conditions. For example, [11] found that the shelf-life of fresh rocket leaves was limited by their appearance score at $5°C$, but by their ascorbic acid content under dynamic temperature conditions.

Generally, the use of specific quality attribute models -as defined by [7]- also entails the determination of the initial value of the selected food quality index: This may not always be feasible and expedient. Although the index might be a quality that can be measured instantly and non-destructively, such as the color of the product, which can be measured easily with a portable spectrophotometer, it may very well be a quality that takes much longer to measure, requires a destructive or invasive procedure, relatively expensive equipment, or a specialized lab environment such as microbial counting, for which a sample needs to be incubated for 1-2 days in a sterilized environment. Without the initial value of the food quality index, the applicability of many kinetic models in the FFV sector would be limited.

Equally important practical challenges also include the real-time determination of FFV pulp temperature non-destructively, as well as exogenous and endogenous factors that affect the deterioration rate of FFVs besides temperature, namely: O_2 and CO_2 concentrations, and the respiratory climacteric phases characteristic of climacteric fruits, both of which cannot be captured by a single secondary model for temperature [12].

The above reasons have instigated research into other smarter methods of food quality monitoring, such as Time-Temperature Indicators (TTIs), which are non-destructive and responsive to the product's surface temperature rather than the ambient temperature. TTIs are small, physical devices in the form of small stickers placed on food packages that change color irreversibly if a threshold temperature is exceeded (partial-history TTIs) or when the cumulative temperature history renders the product unsafe (full-history TTIs). As they only provide visual cues, they do not provide quantitative information about the RSL. A recent review [13] of the commercially-available TTIs shows that all but one are only qualitative indicators. Moreover, the only quantitative indicator simply indicates cumulative temperature exposure and not necessarily the quality or freshness of the product. Without quantitative shelf-life estimates available in real-time, third-order cold supply chain logistics (where actionable insights and decisions are produced and altered in real-time [7]) cannot be implemented.

La Scalia et al. [14] developed a battery-powered Smart Logistic Unit (SLU) that measures temperature, CO_2, relative humidity (RH), and the concentration of Volatile Organic Compounds (VOCs), contains a GPS module, and has network connectivity to post measurements to a database. A shelf-life model was formulated and tested on strawberries based on the linear correlation between VOC level and microbiological growth. In practice, however, many products are shipped in air-tight packaging, making it impossible for such a device to detect the CO_2 or VOCs emitted by such products. In addition, several storage-compatible products are often shipped in a single compartment, in which case, it would be impossible to isolate the contributions of the different products to the total VOCs emitted and measured in the shared headspace. They conducted further experiments on strawberries with their SLU in conjunction with four shelf-life models: A kinetic model with the Arrhenius as a secondary model, a measured-VOCs-based model developed earlier in [15], a measured-CO_2-based model, and a calculated-CO_2-based model [16]. The shelf-life estimates from each of the four models were compared to the true shelf-life determined based on microbiological testing. Although they found the kinetic-Arrhenius shelf-life model to have the smallest percent error, one cannot conclude that the kinetic-Arrhenius model is the best overall, as it is the model which takes the fewest external factors into account: Temperature only. Furthermore, the theoretical soundness of using the Arrhenius model for the shelf-life prediction of food remains a highly divisive issue. Not to mention that air-tight packaging and/or mixing different products in the same storage compartment would render inapplicable any models relying on the direct measurement of gas concentrations. Therefore, a calculated-CO_2-based model seems the most digestible in theory and expedient practice, but [16]'s structuring of that model lacks at least two respects: 1) Aerobic respiration was assumed throughout, which may not always be the predominant mode of respiration under modified atmospheres, and 2) A constant respiratory quotient was assumed- whereas it is generally a function of temperature, storage time, and the concentrations of CO_2 and O_2 [17].

To summarize, third-order cold supply chain logistics require advancing generic shelf-life models, rather than specific quality attribute models. Despite being the most popular, specific quality attribute models are flawed in their theoretical bases, are time-consuming (and sometimes too

expensive) to apply in the last-mile delivery of FFVs, and, most importantly, fail to capture the effects of dynamic environmental factors other than temperature. Generic shelf-life models, in essence, recognize and acknowledge the importance of environmental effects other than temperature, such as VOCs, vibration, moisture loss, and current respiration activity. However, based on our literature review, the following challenges hinder the real-time application of generic shelf-life models in the last-mile delivery of FFVs:

1) The dynamic formation of a local, modified atmosphere due to airtight packaging
2) When measured CO_2 and VOCs are used to track the respiration activity, how would such a model handle a transportation scenario where multiple species of products are being shipped together in the same compartment and sharing the same headspace?
3) The onset of anaerobic respiration in each species when CO_2 gas concentrations reach their maximum tolerable CO_2 limits
4) The changes in respiration rate that occur due to the onset of anaerobic respiration and due to different climacteric phases
5) Estimation of the product's pulp temperature dynamically and non-destructively, since the product's respiration rate is a function of the product's pulp temperature rather than its ambient temperature

Hence, the objective of this study is to establish a generic shelf-life model for FFVs under dynamic logistic conditions that addresses the above five challenges. The model proposed in this paper has been designed such that the effects of instantaneous temperature and CO_2 gas concentration in the local atmosphere are captured without the need for directly measuring the latter. In addition, the model can be applied independently of whether the product is in standard air or a modified atmosphere, shipped alone or with other storage-compatible products.

A. ABBREVIATIONS AND ACRONYMS

List of Abbreviations

1DO	One Door Opening.
3DO	Three Door Openings.
CSL	Consumed Shelf-Life.
FFVs	Fresh Fruits and Vegetables.
IoT	Internet of Things.
PDE	Partial Differential Equation.
QnD	Quick and Dirty.
RH	Relative Humidity.
RSL	Remaining Shelf-Life.
SLEM	Shelf-Life Estimation Model.
SLU	Smart Logistic Unit.
SPC	Statistical Process Control.
SST	Sensor Sampling Time.
TTIs	Time-Temperature Indicators.
VOCs	Volatile Organic Compounds.

List of Abbreviations The next list describes several symbols that will be later used within the body of the document.

List of Symbols

$RSL(t)$	Remaining Shelf-Life (RSL) at time t.
$CSL(t)$	Consumed shelf-life up to time t.
$DR(t)$	Relative decay rate at time t.
$RR(t)$	Product's respiration rate at time t, $[mL\ kg^{-1}hr^{-1}]$.
$RR_o(t)$	Product's respiration rate under optimal storage conditions and standard atmospheric CO_2 concentration of 0.04% at time t, $[mL\ kg^{-1}hr^{-1}]$.
RR_i	Respiration rate at time step i, $[mL\ kg^{-1}hr^{-1}]$.
$symtype$	Symmetry type, 0 for slab, 1 for a cylinder, and 2 for a sphere.
h_i	Surface convection coefficient at time step i, $[W/(m^2 \cdot^\circ C)]$.
Re_i	Reynolds number at time step i.
Nu_i	Nusselt number at time step i.
Gr_i	Grashof number at time step i.
Pr_i	Prandtl number at time step i.
$\mu_{hsair,i}$	Dynamic viscosity of the trapped headspace air, $[kg\ m^{-1}\ s^{-1}]$.
Lc	Characteristic length, which is the radius for a cylinder or sphere, and half the thickness for a slab, $[m]$.
S	Average velocity of the fluid, $[m/s]$.
φ	Macroscopic porosity of bunched leafy vegetable.
SST	Sensor sampling interval $[min]$.
$T(r,t)$	Product's temperature at the radial distance r from the center at time t, $[^\circ C]$.
T_{∞_i}	The ambient temperature at time step i, $[^\circ C]$.
T_{m_i}	Product's midplane temperature at time step i, equivalent to $T(Lc/2, SST \times i)$, $[^\circ C]$.
$T_{s,i}$	Product's surface temperature at time step i, equivalent to $T(Lc, SSt \times i)$,$[^\circ C]$.
k_i	Product's thermal conductivity at time step i, $[W/(m \cdot^\circ C)]$.
$k_{tpair,i}$	Thermal conductivity of trapped air pockets within the bunched product at time step i,, $[W/(m \cdot^\circ C)]$.
k_i'	Effective thermal conductivity of the porous bulk geometry at time step i, $[W/(m \cdot^\circ C)]$.
$k_{hsair,i}$	Thermal conductivity of the trapped headspace air at time step i, $[W/(m \cdot^\circ C)]$.
α_i'	Effective thermal diffusivity of the porous bulk geometry, $[m^2/s]$.
M_{prod}	Mass of the product $[kg]$.
$CO2Mass_i$	Mass of carbon dioxide evolved during time step i, $[g]$.

M_{hsair}	Mass of trapped headspace air in the air-tight container, $[g]$.
M_{tpair}	Mass of trapped air pockets within the bunched product, $[g]$.
$CO2Vol_i$	Volume of CO_2 in the container at time step i, $[mL]$.
$V_{tpair,i}$	The total volume of trapped air pockets within the bunched product at time step i, $[mL]$.
V_{prod}	The product volume, including trapped air pockets.
V_{hsair}	Volume of trapped headspace air, $[mL]$.
$CO2Conc_i$	CO_2 concentration at time step i.
$maxCO2Conc$	Product's maximum tolerable CO_2 concentration in the local atmosphere, above which anerobic respiration begins to dominate.
ρ_{prod}	Product's apparent (bulk) density, $[kg/m^3]$.
$\rho_{tpair,i}$	Density of trapped air pockets within the bunched product at time step i, $[kg/m^3]$.
$\rho_{hsair,i}$	Density of trapped headspace air at time step i, $[kg/m^3]$.
ρ'_i	Effective density of the porous bulk geometry, $[kg/m^3]$.
$c_{p,i}$	Product's specific heat capacity at time step i, $[J/(kg \cdot^\circ C)]$.
$c_{p,tpair,i}$	Specific heat capacity of trapped air pockets within the bunched product at time step i, $[J/(kg \cdot^\circ C)]$.
$c'_{p,i}$	Effective specific heat capacity of the porous bulk geometry at time step i, $[J/(kg \cdot^\circ C)]$.
$c_{p,hsair,i}$	Specific heat capacity of the trapped headspace air at time step i, $[J/(kg \cdot^\circ C)]$.
$\dot{e}_{gen,i}$	Rate of heat generation per unit volume of the product at time step i, $[W/m^3]$.
$\dot{e}_{gen,i,anerobic}$	Rate of heat generation under anerobic respiration, per unit volume of the product at time step i, $[W/m^3]$.
$\dot{e}_{gen,i,anerobic}$	Rate of heat generation under aerobic respiration, per unit volume of the product at time step i, $[W/m^3]$.

III. THEORY AND CALCULATION

The decay rate of an FFV may be accelerated by several factors, such as (1) deviations in temperature from recommended levels, (2) deviations in oxygen, carbon dioxide, ethylene, and Relative Humidity (RH) from the respective recommended levels, and (3) damage due to impact and vibration. Restricting ourselves only to the case of short-lived last-mile transportation, the most influential of those decay factors is most likely to be the temperature and local atmospheric composition, which happen to be, quite possibly, the only decay determinants that could be measured cheaply, non-invasively, and reliably inside the refrigeration compartment. Thus, the following discussion focuses on temperature-driven decay and considers condensation-driven and damage-driven decay to be out of scope.

It is widely reported that the decay rate of an FFV is proportional to its respiration rate [18, p. 71], where the latter is measured in terms of the CO_2 volume evolved per hour per kilogram of product. Since the decay rate can be interpreted as the rate at which the RSL is consumed, we propose the hypothesis that by integrating the decay rate over the elapsed time, the integral should equal, or well approximate, the shelf-life consumed during that time. Should a shelf-life estimation model be built on that premise and proven to be statistically valid, it would be extremely useful for cheap and non-invasive real-time quality monitoring applications. Mathematically, we first begin by defining the RSL at a given time instant t as $RSL(t)$ with (1), which is the difference between the initial estimate of RSL, $RSL(0)$, and the consumed shelf-life up to time t, $CSL(t)$:

$$RSL(t) := RSL(0) - CSL(t) \tag{1}$$

where $RSL(0)$ is set by the distributor based on experience or taken as the maximum shelf-life from handbooks/standards, e.g., [12] and [19] less the time spent since harvest. The problem reduces to computing the CSL up to time t, which is posited to be the area under the curve of the relative decay rate, $DR(t)$, as in (2):

$$CSL(t) := \int_0^t DR(t)\, dt \tag{2}$$

The current decay rate is defined as the ratio of the product's current respiration rate $RR(t)$, to its respiration rate under optimal storage conditions at time t, $RR_o(t)$, under standard atmospheric CO_2 concentration of 0.04%, as in (3). Respiration rates should be ideally sourced from a reliable and accurate experimental dataset with the same cultivar, origin, and maturity at harvest as the modeled product.

$$DR(t) := \frac{RR(t)}{RR_o(t)} \tag{3}$$

Before addressing how $RR(t)$ is calculated, the assumptions on which the proposed Shelf-Life Estimation Model (SLEM) is based should be laid out:

1) An initial shelf-life estimate, $RSL(0)$, is known.
2) There are two possible types of packaging:
   a) Unsealed: The temperature and composition of the local atmosphere around the FFV are no different from the ambient atmosphere. The product exchanges heat with its surroundings either by forced convection if it is in a refrigerated display or natural convection in a room-temperature display. The product may also be in a box with large hole vents, e.g., strawberries in PET clamshell boxes.
   b) Airtight/Sealed: The product is hermetically sealed, which forms a local atmosphere around

the FFV that can differ significantly from the standard atmospheric composition. O_2 levels would decrease, and CO_2 levels would increase due to the product's respiration, creating a modified atmosphere that further inhibits the respiration rate. The product exchanges heat with its local atmosphere by natural convection.

3) For airtight/sealed products, the seal is non-permeable (Perfect seal). The pressure within the sealed package is approximately atmospheric. The packaging boundaries are movable, as is the case with polyethylene bags. Moreover, only CO_2 concentration is tracked by the model and used to predict the onset of fermentation.
4) Non-simultaneous respiration modes: It is assumed that at any time, one of the two modes of respiration (aerobic or anaerobic) is applicable. In reality, a fresh product may utilize the two modes simultaneously, but usually, one is more prominent at a given atmospheric composition [12, p. 24], [20].
5) Optimistic estimate of the RSL: Whenever this is a positive value according to (1), $RSL(t)$ is the time the product would last if the ambient temperature were to return to the product's recommended storage conditions immediately.
6) No exogenous ethylene exposure: The effect of endogenous ethylene is captured by the respiration rate. The effect of exogenous ethylene, however, is not accounted for.
7) Transpiration losses are irrelevant: The effect of moisture loss is only unaesthetic but is not assumed to necessitate spoilage or discarding the product for safety concerns.
8) No freezing or chilling injury
9) No mechanical damage, cuts, or bruises that may be caused by vibration during transportation.
10) Heat conduction between individual fruits/vegetables is negligible.

A. INSTANTANEOUS RESPIRATION RATE

The instantaneous respiration rate $RR(t)$ is the volume of CO_2 gas evolved at time t, per unit mass of the product per unit of time. However, it would be impractical to measure the CO_2 production rate in the refrigeration compartment, as any CO_2 concentration measured would be impossible to isolate for each product in a compartment housing multiple products. Also, some products may be packaged in open packages, while others are in airtight packages that do not allow evolved CO_2 to escape and consequently be detected. Therefore, it is more sensible to calculate - rather than measure - the respiration rate of the modeled product by interpolating on a given dataset of respiration rates under various temperatures, times, and CO_2 concentrations. Other variables that influence the respiration rate, e.g., the presence of cuts, bruises, and vibration level, will be ignored due to the scarcity of experimental datasets that relate those quantities to the respiration rate.

Suppose the products are packaged in unsealed packaging. In that case, the standard atmospheric composition is assumed. Thus, the respiration rate under this condition would become a function of two independent variables (time and temperature). However, if the products are transported in airtight packaging, the CO_2 evolved due to respiration is expected to accumulate and create a locally modified atmosphere, where CO_2 concentration is expected to rise over time. Given an estimate of the volume of air trapped in the airtight packaging, the CO_2 concentration level over time is calculated. In summary, constructing a respiration rate function follows the logic depicted in Figure 1, resulting in two versions of the respiration rate function: One is a function of two variables, and the other of three variables (time, temperature, and CO_2 concentration).

B. PRODUCT's MIDPLANE TEMPERATURE

The dataset underlying the scattered interpolant respiration function in Figure 1 is in terms of the product's midplane temperature, not the ambient temperature, e.g., [21] and [22]. Under a dynamic ambient temperature profile, the temperature below the surface at any moment is seldom equal to the ambient temperature: Fresh products' tissues are mostly water which has a high specific heat capacity, resulting in the product's thermal inertia. As a result, the measured ambient temperature T_∞ must be first converted to the product's midplane temperature T_m before calculating the respiration rate, $RR(t)$. This is possible by solving the one-dimensional, transient heat conduction equation with constant heat generation and constant thermal conductivity:

$$\frac{1}{r^{symtype}}\frac{\partial}{\partial r}\left(r^{symtype}\frac{\partial T}{\partial r}\right)+\frac{\dot{e}_{gen}}{k}=\frac{1}{\alpha}\frac{\partial T}{\partial t} \tag{4}$$

subject to the following conditions:

$$\frac{\partial T(0,t)}{\partial r}=0 \tag{5}$$

$$-k\frac{\partial T(Lc,t)}{\partial r}=[T(Lc,t)-T_\infty] \tag{6}$$

$$T(r,0)=T_m \tag{7}$$

where equations (5)-(7) represent the thermal symmetry, convection symmetry, and uniform initial temperature conditions, respectively. $T(r,t)$ is the temperature at the radial distance r from the center of the sphere, cylinder, or midplane of a slab at time t, α is the product's effective thermal diffusivity, k is the product's effective thermal conductivity, $\dot{e}_{gen}$ is the heat generation rate per unit volume of the product. The value of *symtype*, the symmetry type, depends on the product's geometry, being 0 for a slab, 1 for a cylinder, and 2 for a sphere. h is the surface convection coefficient, Lc is the radial distance from the center of the product to the surface (also called the characteristic length), T_m is the midplane temperature, and T_∞ is the ambient temperature.

A few challenges hinder the direct application of (4) to the transportation context. For instance, T_∞ is time-varying. Also, $\dot{e}_{gen}$ depends on $RR(t)$ and the mode of respiration

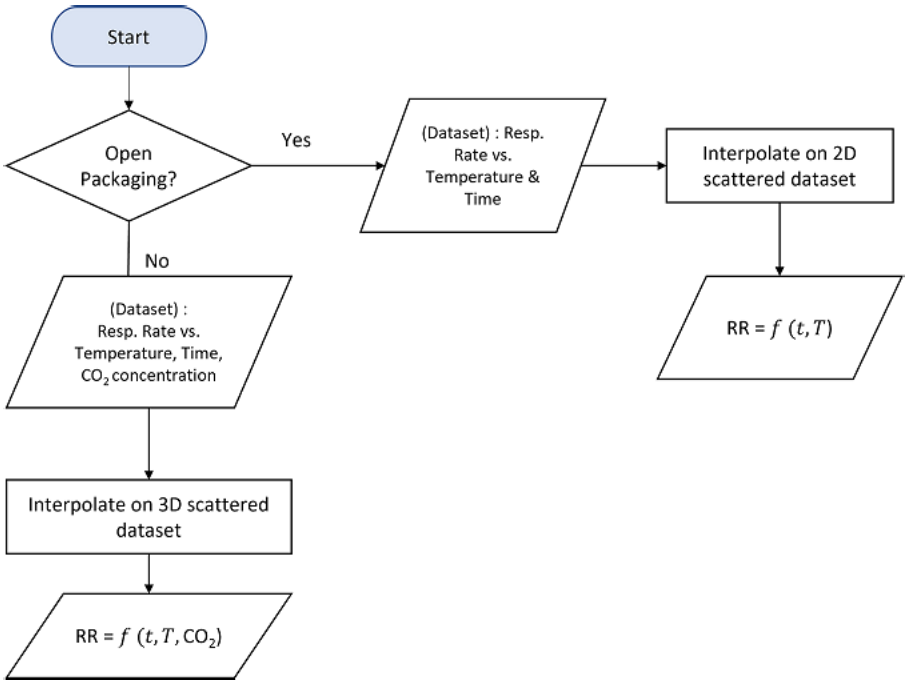

FIGURE 1. Flowchart for constructing the respiration rate function.

(aerobic or anaerobic), as much less energy is released in the latter. Hence, (4) should be solved once for every Sensor Sampling Time (SST). In other words, a temperature profile consisting of m data points would require solving the partial differential (4) m times, where the midplane temperature predicted by the previous solution becomes the initial uniform temperature for the next solution. The loop logic shall follow Algorithm 1, which is provided in detail in *Supplementary File 1*.

C. CO_2 EVOLUTION

If the product is in an airtight package - assuming $RR(t)$ remains constant until the next sampling instant - the volume of CO_2 evolved inside the package during SST minutes is calculated as the product of RR_i, which is $RR(t)$ of the product at time step i, the mass of the product, M_{prod}, and SST. Adding that value to the CO_2 volume in the package at the start of this time step, $CO2Vol_i$, we obtain the incremented CO_2 volume, $CO2Vol_{i+1}$ at the start of the next time step, as per (8).

$$CO2Vol_{i+1}[\,mL] = CO2Vol_i + RR_i\left[\,mL\;kg^{-1}hr^{-1}\right] \times M_{prod}[kg] \times \frac{SST[min]}{60} \tag{8}$$

Consequently, the CO_2 concentration inside the package at the start of the next time step, $CO2Conc_{i+1}$, is the ratio of CO_2 volume at the start of the next time step, $CO2Vol_{i+1}$ to the total volume of air in the airtight package.

Applying the ideal gas law, the mass of CO_2 evolved is calculated as shown in (9).

$$CO2Mass_i[g] = \frac{101325[Pa] \cdot CO2Vol_i[mL] \cdot 44.0095\left[g\;mol^{-1}\right]}{8.314\left[\,J\;mol^{-1}\;K^{-1}\right] \cdot \left(T_{\infty_i}[^\circ C] + 273.15\right)} \times 10^{-6} \tag{9}$$

D. VOLUMETRIC RATE OF HEAT GENERATION

The current volumetric heat generation rate $\dot{e}_{gen,i}$ is calculated based on the mode of respiration. If the current CO_2 concentration is above the maximum tolerable limit, $maxCO2Conc$, (which can be found preferably by experimentation or alternatively, in production guides and handbooks such as [12, p. 24]), anaerobic respiration dominates, and more specifically, fermentation. 2.55 Cal of energy is released per gram of CO_2 released under aerobic respiration, whereas 0.242 Cal is released when the product respires anaerobically by fermentation [23]. Therefore, $\dot{e}_{gen,i}$ is calculated for aerobic and anaerobic respiration per (10) - (11), as shown at the bottom of the next page, respectively.

We make the simplifying assumption that at any instant, the two modes of respiration (aerobic and anerobic) do not overlap. Therefore, $\dot{e}_{gen,i}$ is defined in the model as per (12).

$$\dot{e}_{gen,i} := \begin{cases} \dot{e}_{gen,i,aerobic} & CO2Conc_i \le maxCO2Conc \\ \dot{e}_{gen,i,anerobic} & CO2Conc_i > maxCO2Conc \end{cases} \tag{12}$$

E. TEMPERATURE DEPENDENCE OF THERMOPHYSICAL PROPERTIES

[19, p. 19.3] distinguishes the specific heat capacity of FFVs above and below their initial freezing points. Hence, the current midplane temperature $T_{m,i}$ is compared to the product's highest freezing temperature, and the appropriate value of $c_{p,i}$ is selected accordingly.

[19, p. 19.12] also cites different values of the product's thermal conductivity k_i at different temperatures. Thus, k_i is determined by interpolation in the tabulated thermal conductivity values at $T_{m,i}$.

F. MACROSCOPIC POROSITY IN BUNCHED PRODUCTS

The thermophysical properties of FFVs found in the literature have already accounted for microscopic porosity. However, in the case of bunched leafy vegetables, e.g., bunched spinach or lettuce, there are often trapped air pockets between the leaves of a single bunch or between bunches, as illustrated in Figure 2.

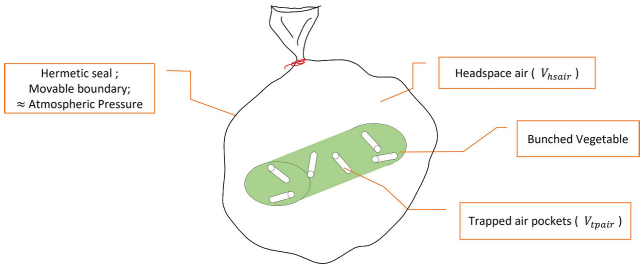

FIGURE 2. Illustration of types of air entrapment.

Macroscopic porosity influences the heat transfer calculations for the product and its overall thermophysical properties. It would not be appropriate to apply (4) to a single leaf with negligible thickness since most of its surface area is in contact with other leaves. This is because the predominant mode of heat transfer to the surroundings of the leaf is conduction rather than convection. As a result, it is more appropriate to consider the entire bunch of leaves as a cylindrical bulk unit. Due to trapped air pockets within the cylindrical bunch, allowance should be made for macroscopic porosity, $\varphi \in [0, 1]$ in Step 17 of Algorithm 1, which we define as the ratio of the initial volume of air pockets $V_{tpair,1}$ to the volume of the porous geometry V_{prod}, as in (13).

$$\varphi := \frac{V_{tpair,1}[mL] \times 10^{-6}[m^3/mL]}{V_{prod}[m^3]} \tag{13}$$

where φ is an input to the model, and V_{prod} is calculated as the ratio of the product's mass M_{prod} to its apparent (bulk) density ρ_{prod}, as in (14).

$$V_{prod}[m^3] := \frac{M_{prod}[kg]}{\rho_{prod}[kg/m^3]} \tag{14}$$

We find the thermal conductivity, specific heat capacity, density, and thermal diffusivity of the porous bulk geometry $\left(k_i', c_{p,i}', \rho_i' \text{ and } \alpha_i', \text{ respectively}\right)$ by considering the classic two-phase mixture problem. Many analytical relations in the literature have been proposed to describe the effective thermal conductivity of a porous material as a function of the solid-phase thermal conductivity k_i, the thermal conductivity of trapped air $k_{tpair,i}$, and macroscopic porosity φ. To find the density of the bulk geometry, ρ_i', the upper bound of the rule of mixtures was used per (15).

$$\rho_i'\left[\frac{kg}{m^3}\right] = \rho_{prod}\left[\frac{kg}{m^3}\right] \cdot (1-\varphi) + \rho_{tpair,i}\left[\frac{kg}{m^3}\right] \cdot \varphi \tag{15}$$

As for the effective thermal conductivity of a porous object, [24] proposed four more relations: Maxwell-Eucken, Landauer's, Russell's, and Ashby's relations, where the recommended use of each depends on the range of values φ lies in and whether the pore phase is connected. Based on their recommendations, k_i' is defined using one of the Maxwell-Eucken, Landauer, or Russell's relations per (16), as shown at the bottom of the next page.

According to [25], $c_{p,i}'$ is computed using (17).

$$c_{p,i}'\left[\frac{J}{kg \cdot^{\circ} C}\right] = \frac{M_{prod}[kg] \cdot c_{p,i}\left[\frac{J}{kg \cdot^{\circ} C}\right] + \frac{M_{tpair}[g]}{10^3[g/kg]} \cdot c_{p,tpair,i}\left[\frac{J}{kg \cdot^{\circ} C}\right]}{M_{tpair}[g] \times 10^{-3}[g/kg] + M_{prod}[kg]} \tag{17}$$

where M_{tpair} is the mass of trapped air within between bunched leaves. As shown in (18), it can be estimated as the product of the initial density of the trapped air pockets,

$$\dot{e}_{gen,i,aerobic}\left[W/m^3\right] = \frac{CO2Mass_i[\,g] \cdot 2.55[Cal/g] \cdot 4.184[\,J/Cal] \cdot \rho_{prod}\left[kg/m^3\right]}{(SST[min] \cdot 60[\,s/\min]) \cdot M_{prod}[kg]} \tag{10}$$

$$\dot{e}_{gen,i,anerobic}\left[W/m^3\right] = \frac{CO2Mass_i[g] \cdot 0.24199[Cal/g] \cdot 4.184[J/Cal] \cdot \rho_{prod}\left[kg/m^3\right]}{(SST[min] \cdot 60[s/min]) \cdot M_{prod}[kg]} \tag{11}$$

$\rho_{tpair,1}$, and the initial estimate of the trapped air pockets' volume, $V_{tpair,1}$:

$$M_{tpair}[g] = \frac{\rho_{tpair,1}[kg/m^3]}{10^3 \left[\frac{kg/m^3}{g/mL}\right]} V_{tpair,1}[mL] \tag{18}$$

The thermal conductivity and specific heat capacity of trapped air pockets viz. ($k_{tpair,i}$ and $c_{p,tpair,i}$) are defined as functions of $T_{m,i}$ (since the air pockets are assumed isothermal with the product) and assuming 100% RH. Hence, humid air properties must be calculated before applying (15), which is addressed in §III-G.

Unless the user provides a single overriding value for the thermal diffusivity of the product, the effective thermal diffusivity for the bulk geometry is calculated by the model for every time step as per (19).

$$\alpha'_i\ [m^2/s] = \frac{k'_i\ [W/(m\cdot^\circ C)]}{\rho'_i \left[kg/m^3\right]\ c'_{p,i} \left[\frac{J}{kg\cdot^\circ C}\right]} \tag{19}$$

The headspace air, by contrast, does not alter the product's thermophysical properties but influences the rate of formation of the modified atmosphere and the calculation of h_i. Thus, the initial volume of headspace air, $V_{hsair,1}$, must be provided by the user if the packaging is airtight. Since the package boundary is assumed to be movable (as most airtight food packages are polyethylene bags), $V_{hsair,i>1}$ will vary with $T_{\infty,i}$ from the initial user-provided value as per the ideal gas law applied in (20).

$$V_{hsair,i>1}[\,mL] = \frac{M_{hsair}[g] * 8.314\left[\,J\ mol^{-1}\ K^{-1}\right] * T_{\infty,i}[\,K]}{28.97\left[\,g\ mol^{-1}\right] * 101325\ [Pa]} \times 10^6 \tag{20}$$

where M_{hsair} can be estimated as the product of the initial headspace air density $\rho_{hsair,1}$, and the initial (user-provided) headspace air volume $V_{hsair,1}$, as in (21).

$$M_{hsair}[g] = \frac{\rho_{hsair,1}\left[kg/m^3\right]}{10^3 \left[\frac{kg/m^3}{g/mL}\right]} V_{hsair,1}[mL] \tag{21}$$

G. HUMID AIR PROPERTIES

Dry air properties significantly differ from humid air [26]. The air inside refrigeration compartments and freezers is usually very humid, with RH values reaching up to 98%. Tsilingiris [27] provides correlations for various thermophysical properties of air as functions of T_∞ and RH, which were applied in our implementation of Step 11 in Algorithm 1 to find the thermophysical properties of headspace air in sealed products and of trapped air pockets within bunched products, specifically: $\rho_{hsair,i}$, $\rho_{tpair,i}$, $\mu_{hsair,i}$, $k_{hsair,i}$, $k_{tpair,i}$, $c_{p,hsair,i}$, and $c_{p,tpair,i}$.

H. SURFACE CONVECTION COEFFICIENT

The surface convection coefficient h is either provided by the user as a single overriding value or calculated from a correlation whose parameters should be provided by the user. Often, literature sources would not provide a single value of h but instead, report empirical equations of the form $Nu = aRe^nPr^m$ for forced convection, where Nu is the Nusselt number, Re is the Reynolds number, Pr is the Prandtl number, a, n, and m are empirical constants. For natural convection, however, an equation of the form $Nu = b\ Pr^m\ Gr^q$ is usually provided instead, where Gr is the Grashof number, b, m, and q are empirical constants. Both types of correlations can be generalized into a Nu-Re-Pr-Gr correlation represented by (22).

$$Nu = aRe^nPr^mGr^q \tag{22}$$

where q is zero in a Nu-Re-Pr correlation, and n is zero in a Nu-Pr-Gr correlation. Single values of h, as well as Nu-Re-Pr and Nu-Pr-Gr correlations compiled from the literature for various products under different modes of cooling and types of packaging, can be found in [19, p. 19.25], Zogzas et al. [28], and [29], for example. Each of the dimensionless numbers on the right-hand side of (22) are calculated as per their definitions in equations (23) - (25).

$$Re_i = \frac{\rho_{hsair,i}[kg/m^3] \cdot Lc[m] \cdot S[m/s]}{\mu_{hsair,i}[kg\ m^{-1}\ s^{-1}]} \tag{23}$$

The i'th Reynolds number is calculated per (23), where $\mu_{hsair,i}$ is the i'th dynamic viscosity of the headspace air, Lc is the characteristic length, and S is the average velocity of the fluid [m/s] (and should be provided by the user for forced convection). Generally, S in a refrigeration compartment varies with time and position [30]. For a domestic refrigerator, the average air velocity is about 0.22 m/s [31]. Nonetheless, the transportation context requires consideration of a refrigerated trailer compartment. The user should consider the least

$$k'_i := \begin{cases} k_i \dfrac{k_{tpair,i} + 2k_i + 2\varphi\left(k_{tpair,i} - k_i\right)}{k_{tpair,i} + 2k_i - \varphi\left(k_{tpair,i} - k_i\right)} & \varphi < 0.15 \\ \dfrac{1}{4}\left[k_{tpair,i}(3\varphi - 1) + k_i(2 - 3\varphi) + \sqrt{\left(k_{tpair,i}(3\varphi - 1) + k_i(2 - 3\varphi)\right)^2 + 8k_ik_{tpair,i}}\right] & \varphi \in [0.15, 0.65) \\ \dfrac{k_i\left[k_i + \varphi^{2/3}\left(k_{tpair,i} - k_i\right)\right]}{k_i + \left(k_{tpair,i} - k_i\right)\left(k_{tpair,i}^{2/3} - \varphi\right)} & \varphi \geq 0.65 \end{cases} \tag{16}$$

ventilated compartment region where products are most prone to spoilage.

The i'th Prandtl and Grashof numbers are defined per equations (24) and (25).

$$Pr_i = \frac{c_{p,hsair,i}\left[\frac{J}{kg\cdot^\circ C}\right]\cdot \mu_{hsair,i}[kg\ m^{-1}\ s^{-1}]}{k_{hsair,i}[W/(m\cdot^\circ C)]} \tag{24}$$

$$Gr_i = \frac{\left(9.81\left[m/s^2\right]\right)\cdot \rho_{hsair,i}{}^2\cdot Lc^3\cdot\left(T_{s,i}-T_{\infty_i}\right)}{\left(T_{\infty_i}[^\circ C]+273.15\right)\cdot \mu_{hsair,i}{}^2} \tag{25}$$

where $T_{s,i}$ is the i'th surface temperature, $c_{p,hsair,i}$, $k_{hsair,i}$, and $\rho_{hsair,i}$ are the i'th specific heat capacity, thermal conductivity, and density of the trapped headspace air, respectively. Since the user provides parameters a, n, m, and q, the right-hand side of (22) is thus determined, and the i'th Nusselt number is found.

Since $h = Nu{\cdot}k_{hsair}/Lc$, then the i'th convection coefficient is:

$$h_i = \frac{Nu_i\cdot k_{hsair,i}\ [W/(m\cdot^\circ C)]}{Lc\ [m]} \tag{26}$$

I. SOLUTION OF THE HEAT CONDUCTION EQUATION

The one-dimensional transient heat conduction equation with constant heat generation is to be solved. Skeel and Berzins [32] provided a numerical solution algorithm for 1-D parabolic and elliptic PDEs that can be used as a library program. It is available in MATLAB as the function called 'pdepe,' which will be used in our implementation to solve the heat transfer problem and referred to hereinafter as *the numerical method*. However, repetitive calls to the function become time-consuming. Performance tests[1] reveal that a single call to this PDE solver for the smallest possible mesh size (3×3 mesh) takes up 2.27 seconds at best. This is problematic when a SLEM is integrated with an optimization engine solving a vehicle routing problem, which would repetitively query the SLEM for various delivery scenarios. For this reason, we devised a 'quick and dirty' approximation or surrogate model to the numerical solution of the PDE using a combination of analytical solutions for situations where computational speed is favored over accuracy. The Quick and Dirty (QnD) approximation method is fully laid out in *Supplementary File 2* as Algorithm 2.

IV. MATERIAL AND METHODS

Samples of three types of fresh products are subjected to pre-defined dynamic temperature profiles until they are observed by the experimenters (through sensory evaluation) to have spoiled. The observed spoilage time is to be compared to the predicted spoilage time output by the SLEM, given the product's properties, packaging condition, and ambient temperature profile.

[1]Conducted on a quiescent machine with an 8th Generation Quadcore 1.60-3.90 GHz CPU and 16 GB RAM.

The three products considered for experimental validation are strawberries (cv. *Elsanta*) in PET Clamshell boxes with large vent holes, bunched red spinach (cv. *Amaranthus dubius*) in sealed polyethylene bags, and apricots (cv. *Prunus armeniaca, L.*) on expanded polystyrene foam dishes.

A. SETUP

The experimental setup consists of a mini-fridge - set to 0°C - placed outdoors, where the outdoor temperature can reach up to 40°C during Summer. The purpose of this setting is to simulate the situation where the refrigeration compartment in a truck is opened to a high-temperature ambiance during loading and unloading events. Once a transportation trip is simulated (by opening and closing the mini-fridge intermittently with the products inside), the products are moved either into an indoor domestic fridge set at 6°C (to simulate refrigerated display at a retailer) or to the indoor kitchen counter at room temperature (to simulate retail showroom display). The temperature to which the products were exposed was logged every 3 minutes using an Efento Bluetooth Low Energy wireless temperature sensor with +/−2°C accuracy connected to a DAQ. However, the sensor did not provide the option of measuring RH, so it was not logged. The ambient temperature logged during the experiments are reported in *Supplementary File 4* as charts and are also available in tabular format in the public data repository available at https://data.mendeley.com/datasets/kphtgxn3ff.

B. DESIGN

Three homogeneous samples from each product were subjected to three different treatments. The products were not washed or moved into different packaging. For each product, the first sample (control) was directly stored at the recommended retail temperature until spoilage without being placed in the outdoor mini-fridge. The second and third samples were placed in the mini-fridge located outdoors for some time to simulate transportation from the distribution center (DC) to the retail center. In the case of One Door Opening (1DO) treatment, the mini-fridge door is opened for 10-15 minutes to simulate product exposure to the hot outside temperature while unloading the truck at a retail center before it reaches the last retailer. In the case of the Three Door Openings (3DO) treatment, the mini-fridge door was opened three times at regular intervals. Finally, the 1DO and 3DO samples were transferred indoors and stored at their recommended retail temperatures.[2]

To judge whether a sample had spoiled, the experimenter visually checked the samples regularly and recorded any signs of spoilage. A sample is declared spoiled for strawberries and apricots when the experimenter first notices white mold. Spinach, however, does not usually spoil by growing fungi but rather by bacterial soft rot, making the leaves wilted

[2]Spinach and strawberries are usually retailed in refrigerated displays at about 6°C, while apricots are retailed at room temperature display at about 25°C.

and saggy. Though the onset of spoilage may begin before mold or sagginess becomes visible to the human eye, visual checking is, nonetheless, the predominant screening method used by end customers to gauge the freshness of the FFV sample they intend to purchase. It is also worth noting that the onset of visible mold will depend on the initial deposition of spores, which varies from field to field and will depend on the cultivation method. This is where the model input $RSL(0)$, i.e., the initial remaining shelf-life, comes in handy. This input, as explained earlier, should be most preferably set by the last-mile distributor based on experience with transporting that species or cultivar and the conditions under which it was cultivated, harvested, prepared, and shipped up until that point in the supply chain. Only in the unfortunate event that a last-mile distributor has no prior experience transporting the product should the midpoint of the shelf-life ranges reported in handbooks or standards be used as a last resort. Table 1 summarizes the test-run settings and the observed spoilage times.

TABLE 1. Experimental treatments and results.

Product	Door openings	Packaging	Mini-fridge temperature	Closed-door durations	Door-open durations (min)	Display temperature	Observed spoilage time (days)
Strawberry	0 (Control)	PET clamshell boxes with hole vents	0 °C	2.3h	0	6°C (in-door fridge)	6
	1 (1DO)			2.3h	15		5
	3 (3DO)			2.3h, 35 min, 35 min	15,15, 15		5
Red Spinach	0 (Control)	Plastic bags	0 °C	2.3 h	0	6°C (in-door fridge)	11
	1 (1DO)			2.3h	15		10
	3 (3DO)			2.3h, 35 min, 35 min	15,15, 15		9.5
Apricot	0 (Control)	Loose on a plate	0 °C	1h	0	25°C (room temperature)	7.18
	1 (1DO)			1h	30		6.30
	3 (3DO)			1h, 1h, 1h	30, 30, 10		5.90

V. RESULTS

Based on the model inputs reported in *Supplementary File 3* (including the respiration rate vs. time and temperature datasets as well as other FFV properties used to initialize the model), the predicted RSLs and error quantities derived using the numerical method are reported in Table 2, while the same is reported for the QnD method in Table 3. We define the model error as the percent deviation of the predicted RSL from the observed RSL. Since the numerical method is presumed to yield the model's most accurate prediction of the RSL and the QnD method being proposed as a surrogate, faster method to potentially substitute the numerical method in real-time applications, the *approximation error* was defined as the percent deviation of the QnD prediction from the numerical method prediction.

Graphical results were extracted from the model in each run. Since 24 graphs were generated by the model for the 12 tests ran for validation (6 runs using the original model and 6 using the surrogate model), they would be too many to report in this manuscript. Therefore, the graphical results have been provided in *Supplementary File 4*. Nonetheless, the graphical output generated for Strawberry (1DO) using the numerical method is shown in Figure 3 and Figure 4 to demonstrate the typical output from the Matlab program.

TABLE 2. Experimental results and error analysis for the numerical method.

Product	Door Openings	Observed RSL (days)	Predicted RSL (days)	Model Error (days)	Model Error (%)
Strawberry	1	5	5.036	0.036	0.72%
	3	5	4.996	-0.004	-0.08%
Red Spinach	1	10	8.679	-1.321	-13.21%
	3	9.5	8.617	-0.883	-9.30%
Apricot	1	6.3	7.104	0.804	12.77%
	3	5.9	7.100	1.200	20.34%

TABLE 3. Experimental results and error analysis for the quick and dirty (QnD) method.

Product	Door Openings	Observed RSL (days)	Predicted RSL (days)	Model Error (days)	Model Error (%)	Approximation Error (%)
Strawberry	1	5	5.01	0.005	0.10%	-0.62%
	3	5	4.94	-0.060	-1.20%	-1.12%
Red Spinach	1	10	7.04	-2.958	-29.58%	-18.87%
	3	9.5	7.00	-2.502	-26.34%	-18.79%
Apricot	1	6.3	7.11	0.815	12.93%	0.15%
	3	5.9	7.11	1.210	20.52%	0.15%

The produced charts plot the time evolution of T_∞ and T_m temperatures, $DR(t)$, $CSL(t)$, and $RSL(t)$. Recall that the model estimates the area under $DR(t)$ curve by trapezoidal integration to obtain $CSL(t)$. The product is considered spoiled when the cumulative integral under the $DR(t)$ graph equals $RSL(0)$. In the following section, the statistical soundness of the model and its behavior across the three products considered in this study are discussed.

VI. DISCUSSION

A. HYPOTHESIS TESTING

In all trials, Samples under 3DO condition were always observed to spoil sooner than those under 1DO. Likewise, samples that experienced any number of prolonged door openings spoiled sooner than the control samples that did not experience any prolonged door openings. A two-factor ANOVA test (without replication) was performed on the observed shelf-lives, where the two factors are the product (Strawberry, Spinach, Apricot) and the treatment (Control, 1DO, 3DO). The ANOVA test results are reported in Table 4.

The p-value for columns in Table 4 is 0.001162, showing that the observed shelf lives across the treatments are significantly different from one another, even at the strict 0.01 significance level. The model agrees with this result, predicting shorter lifetimes for 3DO samples than 1DO samples for all FFVs regardless of the method used (whether numerical or QnD). Another important hypothesis we'd like to test is whether the RSL predicted by the model is significantly different from the observed RSL for each combination of product and treatment. This calls for three more two-factor

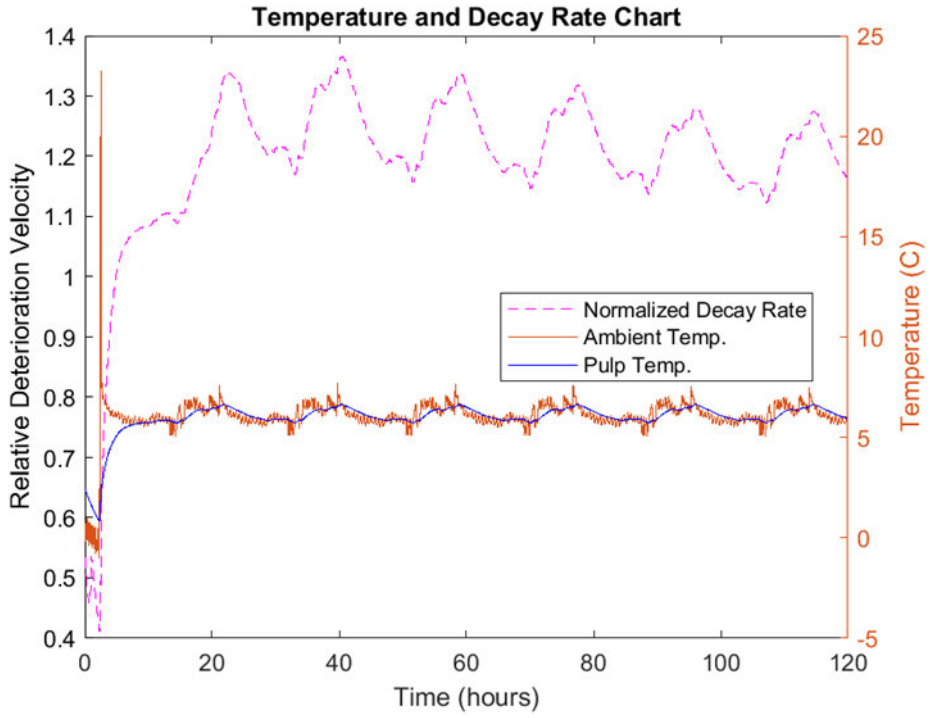

FIGURE 3. Temperature and decay rate for strawberry- sample 1DO - numerical method.

TABLE 4. Results of ANOVA test conducted on observed shelf-lives across different treatments and products.

bfData: Observed Shelf-Lives

	Control	1DO	3DO
Strawberry	6	5	5
Spinach	11	10	9.5
Apricot	7.18	6.3	5.9

bfAnova: Two-Factor Without Replication

SUMMARY	Count	Sum	Average	Variance
Strawberry	3	16	5.333333	0.333333
Spinach	3	30.5	10.16667	0.583333
Apricot	3	19.38	6.46	0.4288
Control	3	24.18	8.06	6.8308
1DO	3	21.3	7.1	6.73
3DO	3	20.4	6.8	5.67

bfANOVA

Source of Variation	SS	df	MS	F	P-value	F crit
Rows	38.36987	2	19.18493	836.5523	5.69E-06	6.944272
Columns	2.5992	2	1.2996	56.6686	0.001162	6.944272
Error	0.091733	4	0.022933			
Total	41.0608	8				

TABLE 5. Results of ANOVA test conducted on observed and predicted RSL (numerical).

bfData: Observed vs. Predicted RSL (Numerical)

	Observed	Predicted
Strawberry, 1DO	5	5.0360
Strawberry, 3DO	5	4.9958
Spinach, 1DO	10	8.6792
Spinach, 3DO	9.5	8.6167
Apricot, 1DO	6.3	7.1042
Apricot, 3DO	5.9	7.1000

bfAnova: Two-Factor Without Replication

SUMMARY	Count	Sum	Average	Variance
Strawberry, 1DO	2	10.036	5.018	0.000648
Strawberry, 3DO	2	9.9958	4.9979	8.82E-06
Spinach, 1DO	2	18.6792	9.3396	0.872256
Spinach, 3DO	2	18.1167	9.05835	0.390109
Apricot, 1DO	2	13.4042	6.7021	0.323369
Apricot, 3DO	2	13	6.5	0.72
Observed	6	41.7	6.95	4.987
Predicted (Numerical)	6	41.5319	6.921983	2.658377

bfANOVA

Source of Variation	SS	df	MS	F	P-value	F crit
Rows	35.92285	5	7.184569	15.59127	0.004536	5.050329
Columns	0.002355	1	0.002355	0.00511	0.945783	6.607891
Error	2.304037	5	0.460807			
Total	38.22924	11				

ANOVA tests, where one test would compare the observed RSL to the RSL predicted by the model using the Numerical method (see Table 5), another test would compare the observed RSL to that predicted by the model using the QnD approach (see Table 6), and the third would inspect whether the predictions made by the model under the Numerical and QnD methods are significantly different from one another (see Table 7).

The p-value for columns in Table 5 (0.945783) is quite large, revealing that the predictions made by the model using the Numerical method are not significantly different from the observed shelf-life, even at the 0.05 significance level. This conclusion supports the validity of the model despite its many simplifying assumptions.

Next, we'd like to assert whether the model's predictions using the QnD method are statistically different from the observed RSL.

The large p-value for columns (0.449737) in Table 6 demonstrates that, once again, predictions made by the model under the QnD method are not significantly different from the observed shelf lives, lending validity to the surrogate model.

Finally, we'd like to check whether the differences between the predictions made by the model under either method (Numerical or QnD) are statistically significant.

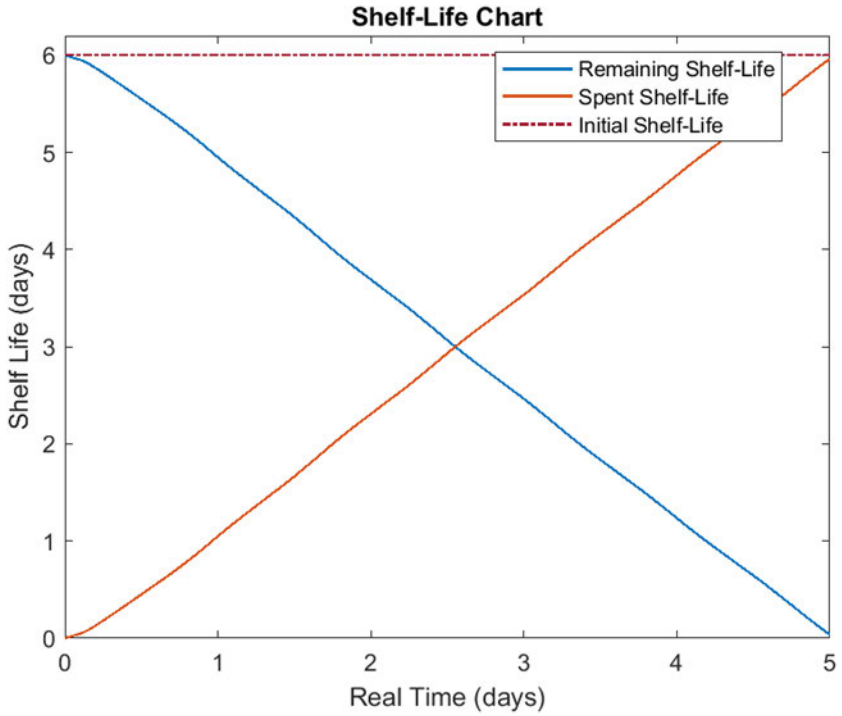

FIGURE 4. Shelf-Life chart for strawberry- sample 1DO - numerical method.

TABLE 6. Results of ANOVA test conducted on observed and predicted RSL (QnD).

bfData: Observed vs. Predicted RSL (QnD)

	Observed	Predicted
Strawberry, 1DO	5	5.0050
Strawberry, 3DO	5	4.9400
Spinach, 1DO	10	7.0417
Spinach, 3DO	9.5	6.9979
Apricot, 1DO	6.3	7.1146
Apricot, 3DO	5.9	7.1104

bfAnova: Two-Factor Without Replication

SUMMARY	Count	Sum	Average	Variance
Strawberry, 1DO	2	10.005	5.0025	1.25E-05
Strawberry, 3DO	2	9.94	4.97	0.0018
Spinach, 1DO	2	17.0417	8.52085	4.375769
Spinach, 3DO	2	16.4979	8.24895	3.130252
Apricot, 1DO	2	13.4146	6.7073	0.331787
Apricot, 3DO	2	13.0104	6.5052	0.732534
Observed	6	41.7	6.95	4.987
Predicted (QnD)	6	38.2096	6.368267	1.171234

bfANOVA

Source of Variation	SS	df	MS	F	P-value	F crit
Rows	23.2342538	5	4.646851	3.074569	0.121586	5.050329
Columns	1.015241013	1	1.015241	0.67173	0.449737	6.607891
Error	7.556913797	5	1.511383			
Total	31.80640861	11				

TABLE 7. Results of ANOVA test conducted on predicted RSLs under numerical and QnD methods.

bfData: Predicted RSL (Numerical) vs. Predicted RSL (QnD)

	Predicted (Numerical)	Predicted (QnD)
Strawberry, 1DO	5.0360	5.0050
Strawberry, 3DO	4.9958	4.9400
Spinach, 1DO	8.6792	7.0417
Spinach, 3DO	8.6167	6.9979
Apricot, 1DO	7.1042	7.1146
Apricot, 3DO	7.1000	7.1104

bfAnova: Two-Factor Without Replication

SUMMARY	Count	Sum	Average	Variance
Strawberry, 1DO	2	10.041	5.0205	0.00048
Strawberry, 3DO	2	9.9358	4.9679	0.001557
Spinach, 1DO	2	15.7209	7.86045	1.340703
Spinach, 3DO	2	15.6146	7.8073	1.310257
Apricot, 1DO	2	14.2188	7.1094	5.41E-05
Apricot, 3DO	2	14.2104	7.1052	5.41E-05
Predicted (Numerical)	6	41.5319	6.921983	2.658377
Predicted (QnD)	6	38.2096	6.368267	1.171234

bfANOVA

Source of Variation	SS	df	MS	F	P-value	F crit
Rows	17.41475	5	3.48295	10.04717	0.012117	5.050329
Columns	0.919806	1	0.919806	2.653341	0.164261	6.607891
Error	1.733299	5	0.34666			
Total	20.06786	11				

Table 7 shows that the differences between the predictions made under either method is also not statistically significant due to the p-value (0.164261), which is larger than the 0.05 significance level.

B. MODEL ACCURACY ACROSS PRODUCTS

Upon inspecting the model errors in Tables 2 and 3, the SLEM is most accurate for strawberries, for which the model and approximation errors are less than 1% and well below +/−1 day. For sealed-bunched spinach, however, the numerical method yielded much more acceptable results than the QnD method, with the former not exceeding 1.5 days in prediction error, while QnD prediction for this case reached 2.9 days in error, possibly due to the length of the spinach experiment, which was almost twice as long as those of strawberries or apricots. Thus, there was more room for approximation errors in QnD calculations to accumulate. Moreover, the sealed and bunched spinach problem involved several sources of error, namely, the assumption of a perfect seal and human error in estimating (1) the exact time the spinach samples were declared to have spoiled (since spinach

leaves spoil less noticeably by wilting as opposed to forming mold), (2) the volume of trapped headspace air V_{hsair}, and (3) the macroscopic porosity φ. It is noteworthy that the model results were exceptionally sensitive to the value of φ. Therefore, we recommend using the Numerical method for estimating the midplane temperature of sealed, bunched leafy vegetables.

As for apricots, both QnD and the Numerical methods performed acceptably well, with a maximum of 1.2 days in prediction error and negligible difference between the predictions made using the two methods. Hence, we have no reservations about using either method for unsealed fruits, whether or not they are climacteric.

It is noted that the SLEM consistently overestimated the RSL for apricots. This is likely due to the apricot's decay rate being accelerated by exposure to exogenous ethylene, which is unaccounted for in the model. Even though the model and approximation errors are high in terms of percentages, they could still be tolerable, considering that they are no more than 1.2 days in error and the fact that a model which accounts for endogenous ethylene production and its interaction with temperature and time is still an improvement over models that do not account for the variation of either endogenous or exogenous ethylene interaction over temperature and time.

VII. CONCLUSION

This paper presented a white-box Shelf-Life Estimation Model (SLEM) implemented in Matlab, which uses any ambient temperature history to estimate the RSL of an FFV in real time. The proposed SLEM was validated experimentally for three fresh products in sealed and unsealed packaging under dynamic temperature profiles. The model performed well with unsealed strawberries and apricots, with errors ranging from 0.04 to 1.2 days in error. The model was exceptionally superior for strawberries, an exemplary non-climacteric fruit.

A surrogate method (QnD) was proposed for computing the pulp temperature for fast, real-time applications, which also produced acceptable results for strawberries and apricots, but performed poorly for bunched and sealed spinach.

Despite simplifying assumptions, the SLEM was found to generate statistically sound predictions nonetheless, which supports the view that the respiration rate and its interaction with time, temperature, and the local CO_2 concentration are the key predictors of decay, notwithstanding the effects of microbiological activity, relative humidity, and exogenous ethylene.

Even though the original and surrogate model results are statistically sound, the surrogate model is not recommended for sealed fresh products or prolonged experiments if prediction errors exceeding 2 days are unacceptable by the end customer.

Although the transportation context was targeted, all key inputs to the model are independent of whether the product is in motion or at rest. Therefore, it can also be applied in cold stores and showrooms for dynamic product pricing and inventory valuation. Another potential application is in vehicle routing problems where the cost of poor quality is to be minimized.

In summary, we consider this model to be a promising solution for quality monitoring and last-mile routing optimization problems. It is non-destructive, non-invasive, and cost-effective as it does not require any additional sensors besides a temperature and humidity sensor.

For future work, some future upgrades may be added to improve versatility, e.g., accounting for the permeability of different types of plastic bags, tracking the levels of O_2 to better predict the onset of anoxia, and the interaction effects between ethylene-generating and ethylene-sensitive products.

ACKNOWLEDGMENT

This paper represents the opinions of the authors and does not mean to represent the position or opinions of the American University of Sharjah.

REFERENCES

[1] S. K. Srivastava, A. Chaudhuri, and R. K. Srivastava, "Propagation of risks and their impact on performance in fresh food retail," *Int. J. Logistics Manag.*, vol. 26, no. 3, pp. 568–602, Nov. 2015.

[2] J. Gustavsson, C. Cederberg, U. Sonesson, R. Van Otterdijk, and A. Meybeck, "Global food losses and food waste," presented at the Save Food Congr., Düsseldorf, Germany, May 2011. Accessed: Jan. 6, 2022. [Online]. Available: https://www.madr.ro/docs/ind-alimentara/risipa_alimentara/presentation_food_waste.pdf

[3] Y. Bouzembrak, M. Kluche, A. Gavai, and H. J. P. Marvin, "Internet of Things in food safety: Literature review and a bibliometric analysis," *Trends Food Sci. Technol.*, vol. 94, pp. 54–64, Dec. 2019. [Online]. Available: http://www.sciencedirect.com/science/article/pii/S0924224419303048

[4] M. Awad, M. Ndiaye, and A. Osman, "Vehicle routing in cold food supply chain logistics: A literature review," *Int. J. Logistics Manag.*, vol. 32, no. 2, pp. 592–617, Apr. 2021, doi: 10.1108/IJLM-02-2020-0092.

[5] G. Hough, *Sensory Shelf Life Estimation of Food Products*. Boca Raton, FL, USA: CRC Press, May 2010. [Online]. Available: https://www.taylorfrancis.com/books/9780429147180

[6] S. Jol, A. Kassianenko, K. Wszol, and J. Oggel, "Issues in time and temperature abuse of refrigerated foods," *Food Saf.*, vol. 11, no. 6, pp. 30–35, 2006.

[7] M. L. Hertog, I. Uysal, U. McCarthy, B. M. Verlinden, and B. M. Nicolaï, "Shelf life modelling for first-expired-first-out warehouse management," *Phil. Trans. Roy. Soc. A, Math., Phys. Eng. Sci.*, vol. 372, no. 2017, Jun. 2014, Art. no. 20130306. [Online]. Available: https://www.ncbi.nlm.nih.gov/pmc/articles/PMC4006170/

[8] M. G. Corradini and M. Peleg, "Shelf-life estimation from accelerated storage data," *Trends Food Sci. Technol.*, vol. 18, no. 1, pp. 37–47, Jan. 2007. [Online]. Available: https://www.sciencedirect.com/science/article/pii/S0924224406002421

[9] M. Peleg and M. G. Corradini, "Microbial growth curves: What the models tell us and what they cannot," *Crit. Rev. Food Sci. Nutrition*, vol. 51, no. 10, pp. 917–945, Dec. 2011.

[10] C. S. Barsa, M. D. Normand, and M. Peleg, "On models of the temperature effect on the rate of chemical reactions and biological processes in foods," *Food Eng. Rev.*, vol. 4, no. 4, pp. 191–202, Dec. 2012, doi: 10.1007/s12393-012-9056-x.

[11] M. L. Amodio, A. Derossi, L. Mastrandrea, and G. Colelli, "A study of the estimated shelf life of fresh rocket using a non-linear model," *J. Food Eng.*, vol. 150, pp. 19–28, Apr. 2015. [Online]. Available: http://www.sciencedirect.com/science/article/pii/S0260877414004506

[12] C. Watkins and J. Nock, "Production guide for storage of organic fruits and vegetables," Dept. Horticulture, Cornell University, New York, NY, USA, Tech. Rep., 10, 2012. [Online]. Available: https://plantpathology.ces.ncsu.edu/wp-content/uploads/2013/12/stored_fruit_veg.pdf?fwd=no

[13] M. Sohail, D.-W. Sun, and Z. Zhu, "Recent developments in intelligent packaging for enhancing food quality and safety," *Crit. Rev. Food Sci. Nutrition*, vol. 58, no. 15, pp. 2650–2662, Oct. 2018. [Online]. Available: https://www.tandfonline.com/doi/full/10.1080/10408398.2018.1449731

[14] G. La Scalia, A. Nasca, O. Corona, L. Settanni, and R. Micale, "An innovative shelf life model based on smart logistic unit for an efficient management of the perishable food supply chain," *J. Food Process Eng.*, vol. 40, no. 1, Feb. 2017, Art. no. e12311. [Online]. Available: https://onlinelibrary.wiley.com/doi/abs/10.1111/jfpe.12311

[15] G. La Scalia, L. Settanni, R. Micale, and M. Enea, "Predictive shelf life model based on RF technology for improving the management of food supply chain: A case study," *Int. J. RF Technol.*, vol. 7, no. 1, pp. 31–42, Jan. 2016. [Online]. Available: https://www.medra.org/servlet/aliasResolver?alias=iospress&doi=10.3233/RFT-150073

[16] R. Sciortino, R. Micale, M. Enea, and G. La Scalia, "A webGIS-based system for real time shelf life prediction," *Comput. Electron. Agricult.*, vol. 127, pp. 451–459, Sep. 2016. [Online]. Available: https://www.sciencedirect.com/science/article/pii/S0168169916304719

[17] K. Tano, A. Kamenan, and J. Arul, "Respiration and transpiration characteristics of selected fresh fruits and vegetables," *Agronomie Africaine*, vol. 17, no. 2, pp. 103–115, Feb. 2009. [Online]. Available: https://www.ajol.info/index.php/aga/article/view/1662

[18] K. C. Gross, C. Y. Wang, and M. Saltveit, *The Commercial Storage of Fruits, Vegetables, and Florist and Nursery Stock* (Agriculture Handbook). Washington, DC, USA: U.S. Department of Agriculture, 2016. [Online]. Available: http://www.ars.usda.gov/is/np/indexpubs

[19] *ASHRAE Handbook—Refrigeration*, American Society of Heating Refrigerating and Air-Conditioning Engineers (ASHRAE), Atlanta, GA, USA, 2018

[20] *Controlled Atmosphere*. Accessed: Sep. 30, 2020. [Online]. Available: https://www.blueatmosphere.nl/controlled-atmosphere/

[21] D. A. Castellanos, J. P. Cerisuelo, P. Hernandez-Muñoz, A. O. Herrera, and R. Gavara, "Modelling the evolution of O_2 and CO_2 concentrations in MAP of a fresh product: Application to tomato," *J. Food Eng.*, vol. 168, pp. 84–95, Jan. 2016. [Online]. Available: https://www.sciencedirect.com/science/article/pii/S0260877415003283

[22] B. Wu, Q. Guo, G.-X. Wang, X.-Y. Peng, J.-D. Wang, and F.-B. Che, "Effects of different postharvest treatments on the physiology and quality of 'Xiaobai' apricots at room temperature," *J. Food Sci. Technol.*, vol. 52, no. 4, pp. 2247–2255, Apr. 2015. [Online]. Available: http://link.springer.com/10.1007/s13197-014-1288-8

[23] K. Wohl and W. O. James, "The energy changes associated with plant respiration," *New Phytologist*, vol. 41, no. 4, pp. 230–256, Dec. 1942.

[24] D. S. Smith, A. Alzina, J. Bourret, B. Nait-Ali, F. Pennec, N. Tessier-Doyen, K. Otsu, H. Matsubara, P. Elser, and U. T. Gonzenbach, "Thermal conductivity of porous materials," *J. Mater. Res.*, vol. 28, no. 17, pp. 2260–2272, Sep. 2013.

[25] A. H. Raval, S. C. Solanki, and R. Yadav, "A simplified heat transfer model for predicting temperature change inside food package kept in cold room," *J. Food Sci. Technol.*, vol. 50, no. 2, pp. 257–265, Apr. 2013, doi: 10.1007/s13197-011-0342-z.

[26] P. T. Tsilingiris, "Thermophysical and transport properties of humid air at temperature range between 0 and 100°C," *Energy Convers. Manag.*, vol. 49, no. 5, pp. 1098–1110, May 2008. [Online]. Available: http://www.sciencedirect.com/science/article/pii/S0196890407003329

[27] P. T. Tsilingiris, "The influence of binary mixture thermophysical properties in the analysis of heat and mass transfer processes in solar distillation systems," *Sol. Energy*, vol. 81, no. 12, pp. 1482–1491, Dec. 2007, doi: 10.1016/j.solener.2007.02.005.

[28] N. P. Zogzas, M. K. Krokida, P. A. Michailidis, and Z. B. Maroulis, "Literature data of heat transfer coefficients in food processing," *Int. J. Food Properties*, vol. 5, no. 2, pp. 391–417, Jul. 2002, doi: 10.1081/JFP-120005794.

[29] R. Earle and M. Earle, *Unit Operations in Food Processing*. Palmerston North, New Zealand: The New Zealand Institute of Food Science and Technology, 2004. [Online]. Available: https://nzifst.org.nz/resources/unitoperations/httrtheory6.htm

[30] M. E. Haque, R. A. Bakar, G. L. Ming, and M. Shakaib, "Predicting airflow and temperature pattern inside a refrigerator through CFD," *ARPN J. Eng. Appl. Sci.*, vol. 11, no. 14, pp. 1–8, Jul. 2016. [Online]. Available: http://www.arpnjournals.org/jeas/research_papers/rp_2016/jeas_0716_4650.pdf

[31] O. Laguerre, "Heat transfer and air flow in a domestic refrigerator," in *Mathematical Modelling of Food Processing* (Contemporary Food Engineering), M. Farid, Ed. Boca Raton, FL, USA: CRC Press, 2010, pp. 445–474. [Online]. Available: https://hal.archives-ouvertes.fr/hal-00583230

[32] R. Skeel and M. Berzins, "A method for the spatial discretization of parabolic equations in one space variable," *SIAM J. Sci. Stat. Comput.*, vol. 11, pp. 1–32, Jan. 1990. [Online]. Available: https://epubs.siam.org/doi/10.1137/0911001

ARWA ABOUGHARIB received the bachelor's degree in mechanical engineering and the master's degree in engineering systems management from the American University of Sharjah, United Arab Emirates, in 2018 and 2020, respectively. She worked as a Graduate Teaching Assistant, from 2018 to 2020, and a Research Assistant, from 2020 to 2021, at her alma mater. Her experience at AUS exposed her to various interdisciplinary research topics, including medical devices, drones, graphene-infused composites, supply chain models, and the design of algorithms for safer fire evacuation from buildings. She enjoys multidisciplinary research and remains passionate about mathematical modeling, simulation, prediction, and optimization of complex physical phenomena and engineering systems. She is also a member of Tau Beta Pi and Pi Tau Sigma engineering honor societies.

MAHMOUD AWAD received the M.S. degree in industrial engineering from the University of Jordan for Science and Technology, Jordan, and the Ph.D. degree in industrial engineering from Wayne State University, USA. He is currently an Associate Professor with the Department of Industrial Engineering, American University of Sharjah. He has been a Certified Six Sigma Black Belt with the American Society of Quality (ASQ) and Ford Motor Company, since 2002. Prior to his academic career, he worked in the industry in USA, Saudi Arabia, and Jordan with Schlumberger Technology Incorporation, Houston, USA, Case New Holland, Chicago, USA, and Ford Motor Company, Dearborn, USA. At Case New Holland, he was one of the six sigma deployment strategy architects and worked as a Quality Manager and a Six Sigma Master Black Belt (MBB). He has published several research papers in international reputed journals and conferences. His areas of research and teaching interests include six sigma, quality and reliability engineering, and reliability centered maintenance. He is currently focused on machine learning and deep learning applications in quality, reliability, and maintenance.

MALICK NDIAYE received the M.S. degree in quantitative methods in economics, optimization, and strategic analysis from the University of Paris 1 Sorbonne, France, and the Ph.D. degree in operations research from the University of Burgundy, France. Before joining the American University of Sharjah, he worked at the University of Birmingham, U.K., and the King Fahd University of Petroleum and Minerals, Saudi Arabia. His recent scholarly work focuses on developing last mile delivery solutions, including vehicle routing optimization in cold supply chains and the use of emerging technologies, such as drones and blockchain, to improve logistics systems. His research interests include operations research, supply chain management, logistics systems, and blockchain technology. He is a Certified Supply Chain Professional with the American Association for Operations Management (APICS).